1044–5110/18/$35.00

COMPUTATIONAL STUDY OF HIGH-PRESSURE LIQUID INJECTION PROCESS BY MEANS OF LES AND PANS APPROACHES

Marija Stipic,[1,*] Branislav Basara,[1] Steffen Schmidt,[2] & Nikolaus Adams[2]

[1]*AVL GmbH List, Graz, 8020, Austria*

[2]*Technical University of Munich, Chair of Aerodynamics and Fluid Mechanics, Garching by Munich, D-85748, Germany*

*Address all correspondence to: Marija Stipic, AVL GmbH List, Graz, 8020, Austria, E-mail: marijas176@gmail.com

Original Manuscript Submitted: 08/07/2023; Final Draft Received: mm/dd/yy

For internal combustion engine, the determination of combustion characteristics and subsequent emissions formation relies heavily on the fuel injection process. With the increasing demand for enhanced fuel efficiency and reduced emissions, it becomes vital to develop fundamental understanding of physical process involved in the fuel injection process. In this study, an optimal numerical approach to predict high pressure liquid injection process in the context of industrial computations has been investigated. In particular, this study focuses on the respective performance of the Partially-Averaged Navier-Stokes and Large Eddy Simulation models to predict turbulent igniting sprays. Both approaches are coupled with widely used Lagrangian Discrete Droplet Method for spray modelling. The results are validated against well established ECN Spray A case in reactive and non reactive conditions. For reacting conditions, Flamelet Genrated Manifold (FGM) combustion model is employed in the present work. Comparative study and validation against experimental data showed that PANS turbulence model allows for coarser grids while still maintaining accurate results.

KEY WORDS: *Engine Combustion Network (ECN) Spray A, Large Eddy Simulation, Partially Averaged Navier Stokes, Tabulated chemistry*

1. INTRODUCTION

Internal combustion (IC) engine remains a significant source of harmful pollution despite the effort made to improve its efficiency and reduce emissions to some extent. To mitigate harmful effects linked to the pollutants emission, transition to cleaner and more sustainable forms of transportation is crucial. Recent European (Hooftman et al. (2018)) and US (Gerard and Lave (2005)) emission legislation dictate stricter emission standards, development of hybrid and electric vehicles, and adoption of alternative fuels. Nevertheless, electrification strategy for medium and large heavy-duty engines, such as engines for cargo ships, heavy-duty trucks and marine engines is still not foreseen. One of the promising concepts for this kind of applications, that has emerged in recent years, is dual fuel engine. The concept of dual fuel combustion has garnered increased interest due to its potential to reduce engine noise, soot and NO_x emissions (Xu et al. (2020)). Additional benefits of dual fuel engines are high fuel flexibility, reliable ignition and combustion as well as robustness. Hence establishing an effective methodology for design of dual fuel engines and its injection equipment represents a key priority.

Multiphase flow mixing and evaporation phenomena are essential in numerous industrial applications, including IC engine. In IC engine, fuel injection is crucial process used to disperse liquid fuel over a wider area of the combustion chamber, thereby increasing the surface needed for more intensive evaporation. Proper fuel injection process is essential for ensuring that the fuel is efficiently and effectively burned, which results in more efficient and stable combustion process leading to better engine performance. Moreover, amount of pollutant emissions released from IC engine strongly depends on the spray process, in particular on fuel atomization and fuel-air mixing process (Petranovic (2016)). As the demand for improved fuel efficiency and reduced emissions continues to grow, detailed understanding of spray processes is essential for the design and optimization of IC engines and fuel injection equipment (FIE). In dual fuel operational mode injector is operated in so called ballistic mode, characterized by short injection duration and high pressure. This leads to more

complex and challenging design process compared to the design of injectors for pure diesel engines. Therefore, effective design of the FIE is considered as crucial step in industrial development of dual fuel IC engines (Gaballa (2023)). To address this challenge, fuel injector manufacturers require advance simulation tools to achieve optimized design for fuel injectors specifically tailored to meet demands of dual fuel engines. Consequently, this leads to improved performance and efficiency of dual fuel IC engines.

Computational fluid dynamics (CFD) tools have been widely used for simulating fuel injection under various operating conditions. However, spray process is highly turbulent and transient process which involves wide range of time and length scales. Moreover, it involves many closely related physical processes such as in-nozzle cavitation, liquid atomization, phase change, mixing and chemical reactions. Consequently, numerical modelling of fuel injection is a challenging task. Several numerical approaches with different level of complexity have been developed to address this problem. For turbulent flow simulations of industrial interest, common practice is to adapt Reynolds-Averaged Navier-Stokes (RANS) turbulence modelling approach due to its low computational cost. However, the range of flow physics that can be accurately represented by RANS models is severely limited. This limitation arises from the fact that RANS models are single-point closures relying on the assumption of self-similarity of turbulence spectrum (Jakirlic et al. (2012)). This assumption implies that entire turbulence spectrum is characterized by only one characteristic turbulent length scale. To overcome these limitations, Large Eddy Simulation (LES) could be employed. LES resolves a wide range of turbulent physics, capturing large coherent structures and significant portion of the inertial scales. Hence, it provides more detailed and accurate description of turbulent flow phenomena, especially in applications where unsteady and complex turbulent structures are essential. However, the increased range of resolved flow physics and high fidelity flow details come at the expense of much greater computational effort (Girimaji and Abdol-Hamid (2005)). Indeed, LES is still prohibitively expensive for engineering applications if only the resolution of the largest scales is needed. With the desire to combine the benefits of RANS and LES methods for complex turbulent flows in practical engineering applications,

the hybrid LES/RANS modelling approaches have been developed. The objective of these models is to extract important large-scale unsteady coherent structures, which dominate the flow, without a burden of resolving inertial scales. Thus, providing accurate predictions in a computationally efficient manner for industrial every day use. One of the hybrid LES/RANS models that has shown capability to accurately and cost-efficiently predict turbulent flow in various canonical flows (see Reyes et al. (2014); Tazraei and Girimaji (2019)) as well as in real-life industrial applications (see Basara et al. (2017); Jakirlic et al. (2012); Krajnović et al. (2012)) is Partially-Averaged Navier-Stokes (PANS) turbulence model. The PANS turbulence model is a scale resolving method that can smoothly vary from RANS to direct numerical simulation based on the model resolution parameters. Compared to RANS models, PANS simulations exhibit improved accuracy due to resolving a portion of turbulent flow. Furthermore, PANS simulations have demonstrated to produce comparable results to LES on coarser computational meshes. Therefore, PANS method is practical and efficient modelling approach for many engineering applications. In this paper, we propose to couple Lagrangian Discrete Droplet Method (DDM) for spray modelling with PANS $k - \zeta - f$ turbulence model for an accurate and computationally affordable 3D CFD simulation of fuel injection process. The Engine Combustion Network (ECN) Spray A is used as a reference case to validate proposed numerical methodology, in both, non-reactive and reactive conditions. Although, this generic geometry differs significantly from a standard production nozzle, it has been widely used for collaborative research and openly accessible data sets with numerical and experimental results are available. For the reactive simulation the Flamelet Generated Manifold (FGM) tabulated chemistry combustion model is employed.

The work presented here is structured as follows. Firstly, the LES Coherent Structure Model (CSM) coupled with DDM is applied to simulate non-reactive and reactive ECN Spray A conditions. The original LES CSM, as developed by Kobayashi (2005) is designed for single phase flow application. Therefore, the model is slightly adapted to obtain better results for two phase flow application. Development of the two phase flow modelling framework is far beyond the scope of the present work. Here a modification to the original formulation of

the LES CSM model is introduced only to obtain better results in cases involving high pressure liquid injection, such as fuel injection in IC engines. This modification of the model is explained in detailed in Section 4.1. Secondly, PANS $k-\zeta-f$ turbulence model is employed to simulate ECN Spray A test case. Numerical study on dependence of the PANS model on the discretization schemes is performed. Additionally, the same test case is simulated utilizing the RANS $k-\zeta-f$ turbulence model. Finally, the proposed DDM PANS simulation methodology is employed to simulate ECN Spray A case in the dual fuel configuration, where methanol is utilized as a primary fuel. The methanol/oxidizer mixture is assumed to be homogeneously mixed in the combustion chamber and the same amount of n-dodecane fuel, as in single fuel configuration, is used to provided required ignition energy. Due to the lack of experimental data for dual fuel conditions this investigation is purely numerical. Obtained results are qualitatively compared to the results of ECN Spray baseline single fuel case and the results obtained from numerical simulation of the same case. The primary objectives of this study are (i) to demonstrate potential of PANS turbulence model to predict high pressure fuel injection process (ii) to propose an effective numerical simulation workflow for development and design of DFIC engines and its fuel injection equipment suitable for every day industrial use.

2. MATHEMATICAL MODEL

The following section will describe, in some detail, numerical models relevant to the present work. Initially, Euler Lagrangian approach for spray modelling along with its sub-models is introduced. Afterwards, the modification of the LES coherent structure model is elaborated. Additionally, a brief explanation of the PANS $k-\zeta-f$ model is provided. Finally, the FGM combustion modelling approach is briefly described.

2.1 Spray Modelling

Spray simulations require simultaneous numerical solution of conservation equations for both, the gas and the liquid phases. With the respect to the liquid phase, for spray calculations in the engineering environment, a commonly used method is a statistical method referred to as the Discrete Droplet Method (DDM). In this method, the dispersed liquid droplets are tracked as Lagrangian parcels within the continuous gas phase, which is represented using Eulerian framework. The parcels represent group of droplets with similar properties such as diameter and velocity. This approach suffers from several limitations which are described in Petranovic (2016); Xue et al. (2014). Nevertheless, it proved to be efficient and accurate in predicting the spray dynamics under turbulent conditions in the industrial development process. To accurately capture spray phenomena with Lagrangian particle tracking method, a set of spray sub-models has to be employed to account for different aspects of spray behavior. These models include primary and secondary breakup, evaporation, wall interaction, atomization, collision and turbulent dispersion. Selection and implementation of these sub-models depends on the specific system and its characteristics. Moreover, the computational cost and accuracy trade-off must be considered to ensure practical and efficient numerical simulation. The present study employs the standard WAVE breakup model of Reitz (1987). Droplet evaporation is modelled with multi-component evaporation approach capable of handling evaporation of droplets composed of arbitrary number of components according to Fink (2005). As the spray droplets pass through the continues gas phase they interact with individual turbulent eddies. This interaction can't be directly resolved by the flow. Hence, the turbulent dispersion model is used. Modification of the spray sub-models for PANS and LES applications is not necessary. The effects of the unresolved scales are assumed to be negligible compared to the droplet interaction with the resolved scales. Hence, for the present PANS and LES simulations, the turbulent dispersion effects are fully covered by interaction of the spray droplets with the scales resolved by the LES or PANS simulation.

2.2 Large Eddy Simulation

The RANS turbulence models are still most commonly used approach in design and optimization process of IC engine due to their efficiency and reliability. However, this approach is limited when it comes to investigating important aspects of combustion process such as cycle to cycle variations and related phenomena. On the other hand, the LES approach enables capturing of cycle-to-cycle variations by directly simulating the large turbulent structures and modeling the influence of subgrid scales on the resolved ones. In the LES framework, set of equations governing the fluid flow are based on the filtered Navier-Stokes equations. Filtering operation is performed to separate the resolved scales of the flow from the unresolved scales. In this work, explicit filtering is not performed, meaning the computational mesh serves as an implicit filter that removes the subgrid scales. Hence, the resolution of the computational grid requires special attention to ensure accurate simulation results. Due to limitations of computational resources, it might not be possible to have fine resolution in the entire domain, but locally where specific phenomena of interest might occur.

The governing equations within the LES framework are given as:

$$\frac{\partial \bar{u}_i}{\partial t} + \frac{\partial \bar{u}_i \bar{u}_j}{\partial x_j} = -\frac{1}{\rho}\frac{\partial \bar{p}}{\partial x_i} + \frac{\partial}{\partial x_j}\left[\nu \frac{\partial \bar{u}_i}{\partial x_j} - \underbrace{(\overline{u_i u_j} - \bar{u}_i \bar{u}_j)}_{\tau_{ij}}\right] \tag{1}$$

where τ_{ij} represents represents the subgrid scale tensor which is modelled according to Boussinesq assumption:

$$\overline{u_i u_j} - \bar{u}_i \bar{u}_j = -2\nu_t \bar{S}_{ij} \tag{2}$$

where ν_t is the turbulent viscosity which is a property of the flow and has to be modelled. Turbulent viscosity is an artificial viscosity, representing equivalent dissipation of unresolved scales of motion Perkovic (2014). In this work, turbulent viscosity is modelled according to Kobayashi (2005). This model is based on coherent structure function which enables avoiding expensive averaging in the homogeneous direction. Another benefit of subgrid scale model based on the coherent structure function is that it doesn't require a wall damping

function of Van Driest type to vanish the eddy viscosity on the wall. The formulation of turbulent viscosity is given in Eq. 3:

$$\nu_{SGS} = C_{CSM}\Delta^2 \left|\bar{S}\right| \tag{3}$$

where the $\left|\bar{S}\right|$ is resolved rate of strain tensor. C_{CSM} is model constant which is locally defined according to following expression:

$$C_{CSM} = C_2 \left|F_{CS}\right|^{3/2} F_\Omega \tag{4}$$

Where F_Ω is energy-decay suppression function given by Eq.5:

$$F_\Omega = (1 - F_{CS}), \tag{5}$$

and F_{CS} is coherent structure function (see Eq. 6) defined as a ratio of second invariant of a velocity gradient tensor Q and the magnitude of a velocity gradient tensor E as defined in Eq.7:

$$F_{CS} = \frac{Q}{E} \tag{6}$$

$$Q = \frac{1}{2}\left(\tilde{W}_{ij}\tilde{W}_{ij} - \tilde{S}_{ij}\tilde{S}_{ij}\right); \quad E = \frac{1}{2}\left(\tilde{W}_{ij}\tilde{W}_{ij} + \tilde{S}_{ij}\tilde{S}_{ij}\right) \tag{7}$$

The resolved velocity strain tensor $\tilde{S_{ij}}$ and resolved vorticity W_{ij} tensor are defined as follows:

$$\tilde{S}_{ij} = \frac{1}{2}\left(\frac{\partial \tilde{u}_j}{\partial x_i} + \frac{\partial \tilde{u}_i}{\partial x_j}\right); \quad W_{ij} = \frac{1}{2}\left(\frac{\partial u_j}{\partial x_i} - \frac{\partial u_i}{\partial x_j}\right) \tag{8}$$

While the C_{CSM} is locally updated parameter based on the local coherence in the velocity field, the C_2 in Eq.4 is fixed model constant with value of $1/22$. This value is obtained from DNS data in non-rotating homogeneous turbulence at the center of turbulent channel flow (Kobayashi (2005)). The performance of CSM model has been well exhibited in variety of idealized and canonical flows. Kobayashi et al. (2008) applied CSM model for simulation of a flow over a backward-facing step and for a flow in an asymmetric plane diffuser, as well as

for staggered jets in crossflow.

In this study, it has been observed that when employing this model in cases involving high-pressure liquid injection, such as in IC engines, the model effectively damps both, eddy viscosity on the wall and in the spray region, where dissipation has its maximum. According to Klein et al. (2019), there is not standard set of governing equations for two-phase flow LES simulation, but rather a variety of different formulations, all with advantages and disadvantages. This paper discuses and analyses suitable closure for eddy viscosity of coherent structure model in the context of fuel injection process. A three dimensional rectangular computational domain with average cell size of 0.25 mm is used to illustrate behaviour of the original coherent structure model. For this purpose n-dodecane is injected into gaseous nitrogen under conditions of 60 bar and 900 K, similarly as in Spray A case. In the Fig. 1 the upper figure shows total eddy dissipation field where it is notable that maximum dissipation occurs in the spray region. The middle figure shows unresolved turbulence representing small scale turbulent motions that are not explicitly resolved by the numerical grid and again the maximum of unresolved energy lies in the spray region. Lower figure shows turbulent eddy viscosity as obtained by coherent structure subgrid model. It can be observed that resulting eddy viscosity is damped in the region of highest dissipation of unresolved scales of motion. Consequently, influence of the unresolved scales on the resolved ones is not captured satisfactorily.

It has been observed, that this leads to overprediction of liquid length and vapor penetration as shown in Sec. 4.1, which in turn results with a wrong prediction of the combustion process. To overcome this issue, a well-established Smagorinsky model with a value of model constant $C_S = 0.1$, is used to obtain eddy viscosity in this case, according to Eq. 9:

$$\nu_{SGS} = \left(C_s f \Delta\right)^2 |S| \tag{9}$$

Where f is a wall damping function of Van Driest type employed to vanish the eddy viscosity

on the wall, thus:

$$f = 1 - exp\left(-\frac{y^+}{25}\right) \tag{10}$$

The obtained eddy viscosity field is then utilized to determine a new value of the coherent structure model constant C_2 from the Eq. 4 and Eq. 3. As it can be seen from the Fig. 2 it appears that a suitable value for C_2 constant in the spray region is unity.

According to Popovac and Hanjalic (2007), damping functions introduce additional non-linearity and often numerical stiffness, which together with dense clustering of the computational grid in the wall-normal direction, may lead to excessive computational cost. On the other had, the coherent structure model is suitable for engineering applications since it accounts for local coherence in the flow without expensive averaging in a homogeneous direction. Additionally, wall-damping function of Van Direst type is not required to vanish eddy viscosity on the wall. Thus to optimize the coherent structure model for wall vicinity and viscous effects in the spray region, in this study it has been proposed to employ a blending function as described in Popovac and Hanjalic (2007):

$$\Gamma = \frac{0.01y^{+4}}{1 + 5y^+} \tag{11}$$

By means of this blending function one can combine two values of C_2 model constant. Namely, in the viscous near wall region where eddy viscosity should vanish, an original value of $C_2 = 1/22$ is kept, and further away from the wall, in the full turbulent field, the C_2 is changed to suitable value which is unity. We now apply the blending principle to the Eq. 3 and obtain a formulation for optimized eddy viscosity within coherent structure model which considers wall effects and local flow properties:

$$\nu_{opt} = \nu_{org}e^{-\Gamma} + \nu_{new}e^{-1/\Gamma} \tag{12}$$

Expression 12 defines optimized, or tuned, turbulent eddy viscosity ν_{opt}, which smoothly varies between original viscosity ν_{org} with $C_2 = 1/22$ near the wall, and ν_{new} defined

with the same equation 3 and 4 but with $C_2 = 1$. This formulation enables blending of the turbulent eddy viscosity between the viscous and fully turbulent definitions utilizing the blending function Γ. Eddy viscosity obtained by this formulation is shown in Fig. 3. It can be seen that the new eddy viscosity has its maximum in the region of highest dissipation of unresolved scales, at the same time the viscosity on the wall is vanished. This formulation is employed to calculate the Spray A case and the results are shown in the Section 4.1.

2.3 Partially Averaged Navier Stokes

The PANS model is a scale resolving turbulence model developed to overcome some of the limitations of traditional turbulence modelling approaches, such as RANS and LES models. Model is envisioned to offer a balance between computational efficiency of RANS models and the accuracy of LES models. The PANS model as proposed by Girimaji et al. (2003) seamlessly vary from RANS to the direct numerical solution of Navier-Stokes equations. The specific closure model used in PANS can vary depending on implementation and application. There are several variants of PANS model derived up to now, throughout this work PANS version based on $k - \zeta - f$ model formulation is used (see Basara et al. (2011, 2018)).

In PANS models, the instantaneous velocity and pressure fields are decomposed into two component, partially filtered component (U_i and P) and unresolved component (u_i and p') as:

$$V_i = U_i + u_i; \qquad p = P + p' \tag{13}$$

After applying filtering operator, which commutes with spatial and temporal differentiation, Navier Stokes equations for partially filtered pressure and velocity fields are written as:

$$\frac{\partial U_i}{\partial t} + U_j \frac{\partial U_i}{\partial x_j} + \frac{\partial \tau\left(V_i, V_j\right)}{\partial x_j} = -\frac{1}{\rho}\frac{\partial P}{\partial x_i} + \nu \frac{\partial^2 U_i}{\partial x_j \partial x_j} \tag{14}$$

The above equation needs closure for the sub-filter stress $\tau(V_i, V_j)$, which takes into account influence of unresolved motion on the resolved flow field. A detailed description on the choice of the closure model can be found in Girimaji (2005). Here we proceed the closure obtained

by using the Boussinesq approximation as:

$$\tau(V_i, V_j) = -\nu_u \left(\frac{\partial U_i}{\partial x_j} + \frac{\partial U_j}{\partial x_i} \right) + \frac{2}{3} k_u \delta_{ij} \tag{15}$$

where ν_u is eddy viscosity of unresolved scales defined as:

$$\nu_u = C_\mu \frac{k_u^2}{\epsilon_u} \tag{16}$$

Additionally, to fully close the system of equations given above, models for unresolved turbulent kinetic energy k_u and unresolved eddy dissipation ϵ_u are needed. A starting point for this development is the RANS $k - \zeta - f$ turbulence model, see reference of Hanjalic et al. (2004). Basara et al. (2011) developed the PANS variant from the $k - \zeta - f$ model due to its excellent near-wall wall behaviour in complex flows. It is important to note that in many industrial applications, the computational cost of wall-resolved LES can be prohibitive due to limited computational resources and time constraints. As described in Basara et al. (2011), the $k - \zeta - f$ model can be effectively combined with universal wall approach, which combines the integration up to the wall with wall functions. Therefore the model is well-suited for enhancing the PANS model. Detailed derivation of the model equations can be found in Basara et al. (2011), here only final form is presented. The equation for unresolved turbulent kinetic energy is defined as follows:

$$\frac{\partial k_u}{\partial t} + U_j \frac{\partial k_u}{\partial x_j} = (P_u - \epsilon_u) + \frac{\partial}{\partial x_j} \left[\left(\nu + \frac{\nu_t}{\sigma_k} \right) \frac{\partial k_u}{\partial x_j} \right] + (U_j - \bar{U_j}) \frac{\partial k_u}{\partial x_j} \tag{17}$$

Eq.17 introduces an additional unclosed term $(U_j - \bar{U_j})$ known as the turbulent transport term, which accounts for the convection of unresolved energy by resolved fluctuations. We use maximum transport model which assumes that transport is directly proportional to eddy viscosity of resolved fluctuations ν_r, for detailed derivation of the possible transport models and its performance see Girimaji (2005) and Murthi et al. (2010). This leads to following

closure and final form of equation for unresolved turbulent kinetic energy:

$$\left(U_j - \bar{U_j}\right) \frac{\partial k_u}{\partial x_j} = \frac{\partial}{\partial x_j}\left(\frac{\nu_r}{\sigma_k}\frac{\partial k_u}{\partial x_j}\right); \qquad \sigma_{ku} = \sigma_k \tag{18}$$

$$\frac{\partial k_u}{\partial t} + U_j \frac{\partial k_u}{\partial x_j} = (P_u - \epsilon_u) + \frac{\partial}{\partial x_j}\left[\left(\nu + \frac{\nu_r}{\sigma_k}\right)\frac{\partial k_u}{\partial x_j}\right] \tag{19}$$

Equations for unresolved eddy dissipation and wall-normal unresolved velocity scale ratio in their final form are defined as follows:

$$\frac{\partial \epsilon_u}{\partial t} + U_j \frac{\partial \epsilon_u}{\partial x_j} = C_{\epsilon 1} P_u \frac{\epsilon_u}{k_u} - C^*_{\epsilon 2}\frac{\epsilon_u^2}{k_u} + \frac{\partial}{\partial x_j}\left[\left(\nu + \frac{\nu_r}{\sigma_\epsilon}\right)\frac{\partial \epsilon_u}{\partial x_j}\right] \tag{20}$$

$$\frac{\partial \zeta_u}{\partial t} + U_j \frac{\partial \zeta_u}{\partial x_j} = f_u - \frac{\zeta_u}{k_u}P_u + \frac{\zeta_u}{k_u}\epsilon_u(1 - f_k) + \frac{\partial}{\partial x_j}\left(\frac{\nu_r}{\sigma_\zeta}\frac{\partial \zeta_u}{\partial x_j}\right) \tag{21}$$

where $C^*_{\epsilon 2} = C_{\epsilon 1} + \frac{f_k}{f_\epsilon}(C_{\epsilon 2} - C_{\epsilon 1})$. The level of physical resolution depends entirely upon model resolution parameters, unresolved to total ratio of kinetic energy f_k and unresolved to total ratio of eddy dissipation f_ϵ. Resolution parameters have values between zero and unity. When the resolution parameters equal unity the PANS model transitions back to its parent RANS model. As the values of resolution parameters decrease more of the turbulent flow structures is resolved. Lastly, in the limit when resolution parameters equal zero, a direct numerical simulation is performed. In this study f_ϵ is set to unity while f_k is specified according to Basara et al. (2018) where a dynamic update of the f_k parameter as a function of cell size is proposed:

$$f_k \geq \frac{1}{\sqrt{C_\mu}}\left(\frac{\Delta}{\Lambda}\right)^{\frac{2}{3}} > \frac{k_u}{k_{tot}} \tag{22}$$

with $\Delta = (\Delta_x + \Delta_y + \Delta_z)^{\frac{1}{3}}$ being cell dimension and Λ an integral length scale. Note that total turbulent kinetic energy required to determine integral length scale is $k_{tot} = k_u + k_r$ and it can be calculated only after the resolved turbulent kinetic energy is obtained. Resolved turbulent kinetic energy is obtained from Eq. 23:

$$k_r = \frac{1}{2}\left(U_i - \overline{U_i}\right)^2 \tag{23}$$

This step involves expensive averaging of the resolved field, as a result this approach is impractical for complex unsteady flow with moving boundaries. Therefore, Basara et al. (2018) further improved this approach by adding transport equation to determine resolved turbulent kinetic, thus supplying the information for the correct cut-off scale. This equation is simply called scale supplying variable (SSV) and it is given by Eq. 24:

$$\frac{\partial k_{ssv}}{\partial t} + U_j \frac{\partial k_{ssv}}{\partial x_j} = (1 - f_k)(P - \epsilon) + \frac{\partial}{\partial x_j}\left[\left(\nu + \frac{\nu_u}{\sigma_{ku}}\right)\frac{\partial k_{ssv}}{\partial x_j}\right] \tag{24}$$

Finally, by continuous calculation of both, unresolved and resolved turbulent kinetic energy, assuming that $k_r = k_{ssv}$, f_k parameter is efficiently specified in every cell at the end of every time step depending on the flow conditions and mesh resolution.

With a desire to accurately depict high-pressure fuel injection with conditions relevant to Diesel engines under minimal computational effort the PANS $k - \zeta - f$ SSV model is employed in this work. The PANS simulation results of ECN Spray A test case are compared to experimental data and LES simulation in Section 4.2.

2.4 Flamelet Generated Manifold

As already stated in Section1 of this paper, the primary goal of this study is to establish accurate, and for today's industry, computationally affordable numerical methodology to predict fuel injection process relevant for IC engines. Due to the inherent complexity of diesel combustion which includes thousands of species and tens of thousands of chemical reactions between them, computational power that is necessary quickly grows beyond practical limits, especially in the industrial environment (Tvrdojevic et al. (2019)). Hence, to minimize computational effort, the Flamelet Generated Manifold (FGM) tabulated chemistry model is employed to describe chemical kinetics. The model is presented in van Oijen et al. (2016) as a practical and efficient method for accurate combustion modelling under reduced computational cost compared to detailed chemistry simulation. This model allows for separate computation of flow and flame structure by assuming that a turbulent multi-dimensional flame

can be represented as a collection of locally one-dimensional flamelets, and that the chemical scales are significantly smaller than the turbulent scales. This involves pre-computing combustion chemistry using detailed chemical mechanism of any desired level of complexity. The resulting thermochemical data of the flamelets are then stored in a lookup table, which is subsequently utilized to interpolate the data during the CFD simulation. In this study lookup table is generated using AVL TABKIN™ table generation tool based on perfectly stirred reactor (PSR) simulations carried out at constant pressure conditions. More details about TABKIN™ generation tool can be found in FIRE™ (2022b). All thermochemical data obtained from PSR simulations are stored in the lookup table as a function of two independent variables, progress variable and mixture fraction, for which transport equations are solved during CFD simulation. The mean general transport equation for control variables reads:

$$\frac{\partial \bar{\rho}\tilde{\phi}}{\partial t} + \frac{\partial \bar{\rho}\tilde{u_i}\tilde{\phi}}{\partial x_i} = \frac{\partial}{\partial x_i}\left(\bar{\rho}\left(D + D_T\right)\frac{\partial \tilde{\phi}}{\partial x_i}\right) + \overline{\dot{\omega}_\phi} \tag{25}$$

where ϕ represents either progress variable or mixture fraction. Here, $\tilde{u_i}$ denotes Favre averaged or filtered velocity component. For more detailed description of software implementation see FIRE™ (2022a). The progress variable represents the progress of the combustion reaction and it is defined as scalar that varies between zero (unburnt) and unity (burnt). It quantifies the degree of fuel consumption and provides a measure of the local flame position. The mixture fraction is a scalar quantity that also varies between zero and unity, where zero represents pure oxidizer and unity represents pure fuel. It characterizes mixing process in turbulent combustion. In this study, turbulent flow field is resolved by adopting LES, PANS and RANS turbulence models, which depending on the modelling approach results in unresolved subfilter scales. To account for influence of turbulence on combustion a ß-Presumed Probability Density Function (PPDF) averaging approach is performed over control variables and its variances. General transport equation for control variable variances is defined as:

$$\frac{\partial \bar{\rho}\tilde{\phi}_{var}}{\partial t} + \frac{\partial \bar{\rho}\tilde{u_i}\tilde{\phi}_{var}}{\partial x_i} = \frac{\partial}{\partial x_i}\left(\bar{\rho}\left(D + D_T\right)\frac{\partial \tilde{\phi}_{var}}{\partial x_i}\right) + 2\bar{\rho}D_T\left(\frac{\partial \tilde{\phi}_{var}}{\partial x_i}\right)^2 - \bar{\rho}\tilde{\chi}_\phi \tag{26}$$

where $\tilde{\chi}_\Phi$ is scalar dissipation rate defined as follows:

$$\tilde{\chi}_\Phi = 2\frac{\epsilon}{k}\tilde{\phi}_{var} \tag{27}$$

In case of premixed combustion regime, averaging is performed over progress variable, while for non-premixed cases over mixture fraction. ECN Spray A is application featuring non-premixed combustion conditions. Hence, in this study ß-PPDF averaging over mixture fraction is adopted. Nevertheless, dual fuel conditions require simultaneous consideration of premixed and non-premixed combustion regimes. Therefore, for dual fuel simulation turbulence chemistry interactions were considered over both, progress variable and mixture fraction. Additionally, the lookup table generated for dual fuel simulation has one dimension more compared to table used for single fuel simulation, specifically the fuel composition parameter.

3. DESCRIPTION OF THE SIMULATED TEST CASE

The test case used for validation of proposed methodology is the Engine Combustion Network (ECN) Spray A which features typical operating conditions of diesel engines. Detailed specifications on this experiment are available at ECN (2023). Main operating conditions are summarized in Table 1. The ECN experimental database of the nonreactive and reactive conditions is used to validate numerical results.

Additionally in the present work, the ECN Spray A is configured for dual fuel conditions. Due to the lack of experimental data for dual fuel configuration, results were qualitatively compared to single fuel case and other numerical studies. Similar study can be found in Gaballa (2023), where two-phase Real Fluid Model (RFM) has been applied to study evaporation and mixing in dual fuel configuration. In the work of Xu et al. (2020) a numerical study on effects of ambient methanol on pollutants formation in dual-fuel spray combustion can be found. The ECN Spray A condition was selected because it closely represents the typical operating parameters of modern dual fuel internal combustion engines. Although, it

is not a direct representation of the dual fuel configuration, it serves as a reasonable starting point for studying and understanding dual fuel combustion process. For that purpose non-reactive and reactive ECN Spray A baseline condition is investigated in dual fuel configuration, where methanol is utilized as a primary fuel. The methanol/oxidizer mixture is considered to be homogeneously mixed and has equivalence ratio of 0.3, corresponding to medium-load conditions in dual fuel engine (Xu et al. (2020)). The initial pressure is slightly modified in such way that the initial ambient density of 22.8 kg/m^3 is maintained.

3.1 Computational domain and numerical setup

The computational domain, shown in Fig. 4, is a cubic hexahedral mesh, with the same characteristic dimensions as experimental device. The maximum cell size is 1 mm, located mainly outside of the spray area, 3 refinement levels are employed in the spray region while for the liquid core 4 refinement levels are performed. The resulting mesh has a minimum cell size of $62.5\mu m$ in the liquid core and total number of cells in the computational domain is 14 594 828.

The AVL FIRE^{TM} 3D-CFD solver has been adopted to perform spray simulations under realistic engine conditions. The solution method is based on the fully conservative finite volume approach with all the dependent variables evaluated at the center of the control volume. The method allows any type of the computational meshes. The overall solution procedure is iterative and based on the combination of SIMPLE algorithm and PISO corrections. The temporal discretization method is based on the first-order accurate Euler implicit scheme. To obtain a value at the cell-face center, a second order linear approximation is used. A second order midpoint rule is used for integral approximation. For solving convection a variety of differencing schemes is employed. For turbulence, energy and species transport equations, first order upwind differencing scheme was employed. The continuity equation is discretized utilizing central differencing scheme. In case of LES and RANS simulations for the momentum equation MINMOD (see Sweby (1984)) differencing scheme is used. It has been reported in Basara et al. (2011) that when the unresolved turbulence as modeled by

PANS model is small, applied differencing scheme on the momentum equation is getting to be of higher importance. Therefore, in this study we apply upwind, central, MINMOD and AVL SMART (see Przulj and Basara (2001)) schemes for the momentum equation to investigated influence of numerical schemes on the PANS simulation results. See the comparison in the Section 4.2.

The FGM lookup table is generated utilizing a hybrid reduced n-dodecane mechanism (Lapointe et al. (2019)) which considers 65 chemical species and 363 elementary reactions, the mechanism is available at (LLNL (2022)). The table discretization is summarized in the Table 2. Table is discretized in such way that the higher refinement is obtained at the most reactive conditions, considering n-dodecane auto-ignition. Fuel ratio and progress variable variances are dimensions which are employed in the table only for the dual fuel configuration.

In Fig. 5, the 3D CFD simulation workflow used in this study to calculated high-pressure liquid injection process is summarised.

4. RESULTS AND DISCUSSION

The obtained numerical results are validated against experimental data such as vapor penetration, liquid length, gas velocity and mixture fraction in radial and axial direction, as well as ignition delay time. All of the values are calculated as recommend by (ECN). Following ECN recommendations are considered: the vapor penetration is defined as the maximum distance from the nozzle outlet to the point where the fuel mass fraction is 0.1%. The liquid length is defined as maximum distance from the nozzle outlet to the farthest axial position where projected liquid volume in the cross-stream direction decreases to $0.2e-3mm^3$ liquid per mm^2. The projected liquid volume is $PLV = \int LVFdy$, where LVF is the liquid volume fraction. Finally, high temperature ignition delay time is defined as the time of maximum gradient $\frac{dT}{dt}$ in temperature.

4.1 Model validation: LES

Firstly, numerical results obtained from LES simulation utilizing the blending function as described in Section 2.2 are compared to the results obtained from original LES coherent structure model as well as to the experimental data. The Fig. 6 shows comparison for liquid length and vapor penetration. As visible from the Fig. 6 results obtained utilizing blending function for turbulent eddy viscosity resulted with improved results in terms of both, liquid and vapor penetrations. The liquid length reported by the original LES CSM model with the constant value of $C_2 = 1/22$ is significantly overestimated. In addition, vapor penetration predicted by non modified LES CSM model is over-predicted. Modifying turbulent eddy viscosity within LES CSM model resulted with liquid and vapor penetration that fairly agree with experimental data. This can be attributed to the fact that we increased the turbulent eddy viscosity of the gaseous phase in the spray region and thus enable the liquid to exhibit longer penetration length, while the original formulation of the LES CSM model is somewhat over-diffusive. This behavior can be seen in Fig. 7 and Fig. 8 where eddy viscosity of the original model and that obtained from the new formulation are shown, for the time instances of 0.1 and 1 ms, respectively. It is notable that keeping the C_2 at the constant value of $1/22$ in the entire numerical domain results with damped eddy viscosity in the spray region. The low eddy viscosity of the gaseous phase implies minimal to no resistance to liquid penetration. As a result, the original model formulation tends to overestimate both, the liquid and vapor penetrations. Introducing the blending function to combine two values of C_2, $1/22$ in the outer edge of the domain and 1 in the spray region resulted with increased values of eddy viscosity in the spray region where the dissipation of the unresolved scales is the highest. However, even with modified eddy viscosity an over-prediction of the liquid tip in the initial stage of the spray is notable in the Fig. 6.

Additionally, comparison of the radial distribution of n-dodecane mass fraction obtained from two LES simulations and experimental measurements is shown in Fig. 9. Comparisons are made at 18, 30 and 40 mm from the nozzle outlet. Numerical results are time averaged in the interval between 1.5 and 3 ms. Once again, the simulation results obtained from LES

simulation with modified eddy viscosity are in better agreement with the experimental profile of the mixture fraction. The simulation results agree reasonably with the experimental data in terms of transversal distribution of the mixture fraction along the radial direction. However, the peak values of the mixture fraction on the jet axis are not captured satisfactorily. Based on this results, it can be deduced that, employed numerical mesh resolution is inadequate to accurately capture involved physical phenomena and the main features of the spray. Possible reason for this is higher diffusion caused by the big cell surface, which is directly reflected in the accuracy of the results obtained by the LES approach (Žilić (2021)). Instead of refining the computational mesh to improve accuracy of the results in this study, a PANS turbulence model is applied as an efficient alternative to the LES models.

4.2 Model validation: PANS

As reported by Basara et al. (2011), turbulence models with variable resolution, such as PANS model, pose a challenge to numerical schemes. In regions with the coarse resolution, the computational behavior of the PANS model resembles that of RANS, and the choice of the numerical scheme prioritizes computational robustness. Typically, RANS models utilize second-order upwind schemes, for example MINMOD. Conversely, in regions with fine resolution, PANS model requires computational capabilities similar to LES. In the present work, we perform PANS computations employing first-order upwind scheme, second-order MINMOD, AVL SMART and central differencing schemes for the momentum conservation equation, and compare their results. Fig. 10 and Fig. 11 show comparison of the liquid length and vapor penetration predicted with PANS simulations using different numerical schemes. The best agreement with experimental data is obtained with MINMOD and AVL Smart differencing schemes. Employing upwind scheme produced nonphysical peak in the initial stage of the spray, while after 0.25 ms predicted liquid length converged to the experimental curve. Additionally, a small overestimation of the liquid length predicted by simulation with central differencing scheme is visible.

The reason for the differences in predicted liquid length and vapor penetration can be

attributed to different numerical dissipation and diffusion properties of the employed differencing schemes. These properties can affect the ability of the numerical method to accurately capture dynamics of turbulent flow, and how the small modeled scales fluctuations interact with the resolved scales. The choice of numerical scheme can effect the accuracy and fidelity of the results. Fig. 12 and Fig. 13 show temperature and equivalence ratio distribution as predicted by PANS simulations employing different numerical schemes. As visible from the presented results upwind scheme introduced excessive numerical diffusion, which damped the small scale turbulent fluctuations and led to an over smoothing of the turbulent flow. On the contrary, pure central scheme doesn't introduce smoothing. Additionally, due to insufficient dissipation it can result with numerical instability and nonphysical oscillations (Ferziger and Peric (2002)). Thus as visible from the temperature and equivalence ratio distribution in Fig. 12 and Fig. 13 the predicted two phase interface is artificially over sharpened. Both the MINMOD and SMART methods exhibit second-order accuracy on refined grids and show robust convergence properties. However, it is worth noting that compared to the MINMOD method, the SMART method is characterized by lower numerical diffusivity and therefore higher accuracy especially on coarser grids. Our results clearly show that the SMART scheme reproduces the expected fine-scale flow structures much more distinctly for a given grid resolution. As a result, all PANS simulation results presented in this paper use the AVL SMART differentiation scheme, while the LES results were derived using the MINMOD scheme.

In Fig. 14 PANS model resolution parameter, total, resolved and unresolved turbulent kinetic energy are shown. It is visible that maximum value of the resolution parameter lies in the region close to the nozzle exit, indicating that this part of the flow can't be resolved by the employed mesh resolution. Hence, in the cells where resolution parameter equals unity, PANS model will reduce to its parent RANS model and turbulent flow will be completely modeled. As a result, adequate description of the dense spray region is preserved, despite insufficient mesh resolution for resolved simulation in this region. Correspondingly, maximum of unresolved turbulent kinetic energy lies in the region where values of resolution parameter

are high. Contrary, maximum of the resolved energy is where resolution parameter has lower values. Total turbulent kinetic energy is obtained by summing up resolved and unresolved turbulent kinetic energy.

Fig. 15 shows the liquid length and vapor penetration obtained with PANS simulation and compared to the results obtained from LES simulation with the blending function. It can be seen that PANS simulation exhibited better agreement with experiment compared to LES. This can be attributed to the fact that PANS model is designed to be adaptive, meaning it can transition smoothly from completely modeled to partially resolved regions, based on the the gird resolution and the local flow conditions. As already seen in the Fig. 14, grid resolution in the region close to the nozzle exit is insufficient to resolve turbulent flow structures of this flow. Therefore, PANS model showed its benefit of retrieving its parent RANS model equations and completely modelling this region of the flow. Consequently, PANS model outperformed LES on this particular mesh for given flow conditions. Comparison of the gas velocity and the mixture fraction axial distribution as predicted by LES simulation with blending function and PANS simulation to experimental data is shown in Fig. 16. Results obtained from PANS simulation appear to be in better agreement with experimental data compared to the LES results. It can be seen that gas velocity close to the nozzle exit is overestimated by LES, while PANS result shows a good agreement with experimental profile. In addition, axial distribution of the mixture fraction is well captured by PANS simulation.

Additionally, radial distribution of the mixture fraction at 18, 30 and 40 mm from the nozzle exit as obtained from LES and PANS simulations is compared to the experiment in Fig. 17. For all three distances from the nozzle exit mixture fraction distribution as predicted by PANS simulation is in better agreement compared to the mixture fraction distribution predicted by LES simulation. The predicted peak values and radial distribution of the mixture fraction obtained by PANS simulation agrees reasonably well with experimental profile.

In Fig. 18 temperature distribution as obtained by LES simulation with blending function, RANS $k-\zeta-f$ simulation and PANS $k-\zeta-f$ simulation is shown. All three simulations reported similar temperature range and peak temperatures values. In addition predicted

distance from the nozzle exit where the mixture ignites is similar in all three simulations. However, RANS simulation predicted considerably longer flame penetration, while PANS simulation is in agreement with LES result. The same comparison is made for equivalence ratio distribution in Fig. 19. All the results appear similar, in terms of equivalence ratio values. It should be noted from the presented results that predicted temperature and equivalence ratio field obtained from the RANS simulation is very smooth, and no fluctuations or small scale structures are visible. On the other hand, PANS results show much more fine scale structures due to resolving portion of the fluctuating scales. Comparing the PANS results with LES results on the same mesh, it can be seen that PANS delivered the same level of detail in terms of resolving portion of the turbulent flow. However, PANS simulation exhibited more accurate results than LES when compared to experimental data.

4.3 Dual fuel configuration

Current section presents the results of ECN Spray A baseline case in dual fuel configuration. This case is calculated employing PANS turbulence model. In the Fig. 20, liquid length and vapor penetration between the single fuel and dual fuel configuration is shown. The obtained results are in agreement from the findings of Gaballa (2023), where it has been shown that the gaseous phase doesn't have high influence on the penetration length of the liquid phase. As can be seen from the obtained results, both liquid and vapor penetrations of dual fuel case are very similar to the single fuel case. However, presence of the methanol is expected to have significant influence on the combustion process characteristics, such as ignition delay time and pollutant formation rates. Indeed, different fuel mixtures have significant influence on the ignition delay time. It has already been shown in many experimental (see Schlatter et al. (2012); Xu et al. (2022)) and numerical (see Eder et al. (2018); Xu et al. (2020)) studies that the presence of the lean premixed high-octane fuel retards the ignition delay time of the directly injected high-cetane fuel. In addition, the delay of ignition becomes more apparent when the ambient temperature decrease (Xu et al. (2020)).The behaviour of ignition delay time for different different ambient temperatures in single and dual

fuel configuration of ECN Spray A case is shown in Fig. 21. The from the PANS simulation obtained ignition delay time for ECN Spray A baseline case at the temperature of 900 K is accurately predicted comparing to the ignition delay time measured in experiment. It can be seen that ignition delay time of the dual fuel case for the same ambient temperature is significantly longer. In addition, as the ambient temperature increases ignition delay time of both single and dual fuel case decreases, which is in line with other relevant findings available in the literature. Longer ignition delay time in dual fuel case results with longer time for mixing before high-temperature combustion starts (Xu et al. (2020)). Consequently, as it can be seen from the Fig. 22, dual fuel case exhibits locally lower temperatures compared to the single fuel case. In addition, equivalence ratio of the dual fuel case is lower in the high fuel region compared to the single fuel case, shown in Fig. 23. Lower equivalence ratio is beneficial for soot reduction (Xu et al. (2020)), while lower local temperatures are beneficial for NO_x reduction (Alla et al. (2000)). The spacial distribution of OH mass fraction plays important role in indicating start of the high temperature combustion, while the HCHO mass fraction distribution is indicator of low-temperature ignition delay. Fig. 24 and Fig. 25 show the comparison of OH and HCHO mass fraction spatial distribution for single and dual fuel case, respectively. The highest distribution of OH in the single fuel case is found along the stoichiometry line, while for the dual fuel case OH appear to be distributed over wider range of the stoichiometry line. The mass fraction of HCHO is relatively higher and wider spread out in terms of spatial distribution for single fuel case. For the dual fuel case HCHO is mostly found close to the nozzle exit. All of the presented results are consistent with the above stated fact that methanol retards ignition of the n-dodecane spray. Additionally, scatter plots with HCHO mass fraction as color map, and the temperature and equivalence ratio as axes are prepared. The Fig. 26 shows scatter plots prepared from the results obtained from the PANS and LES simulation for the single fuel case, as well as PANS simulation for dual fuel case. Results from LES and PANS simulation for single fuel case are very similar, both of them yield the highest mass fractions of HCHO in the subspace of temperature between 750 K and 1250 K, and equivalence ratio between 3 and 8. Comparing the scatter plots

of dual fuel case to the single fuel case it can be observed that dual fuel strategy reduced equivalence ratio of the pilot fuel spray in the high temperature region.

5. CONCLUSION

The main objective of this work was to propose a reliable and efficient CFD simulation workflow for two-phase simulation in the context of dual fuel internal combustion engine. To this goal, present study investigated performance of different numerical approaches to simulate high-pressure fuel injection with the respect of industrial requirements. LES turbulence modelling approach with a subgrid model based on the coherent structure function and the scale resolving PANS turbulence model have been coupled with Euler Lagrangian Discrete Droplet Method for spray modelling. In comparison to the well-established and viable turbulence modelling technique of LES for single-phase flow, the application of LES to two phase flows is still at the early stage of the development. Therefore, a modification to the original LES coherent structure model has been introduced to improve a prediction of high-pressure liquid fuel injection process. The modification is based on a blending function used to tune the turbulent eddy viscosity for two-phase application. The new formulation of eddy viscosity enables smooth transition from viscosity defined for near wall region to viscosity appropriate for turbulent region. Viscosity formulation in the near wall region is kept the same as in the original model with the same model constant. For the fully turbulent region the value of the model constant is changed.

In this study ECN Spray A benchmark case, in both reactive and non-reactive conditions, was utilized to validated proposed modification of LES coherent structure model and to investigate the performance of the PANS turbulence model. The modified LES model showed improved results of predicted liquid and vapor penetrations, and mixture fraction distribution, compared to the original model formulation. However, the PANS turbulence model outperformed the results of LES on the same computational mesh. The generated computational mesh is designed to be computationally affordable for everyday industrial use. However, this compromises the mesh resolution, rendering it insufficient for proper LES calculation. On

the other hand, PANS model can provide good compromise by gradually transitioning from RANS in regions where grid resolution is coarser to partially resolving the flow in in regions the grid is sufficiently fine. This feature allowed PANS model to maintain accurate predictions for coarser grids compared to the ones required for proper LES calculation. Some potential improvements of the results from both, LES and PANS, involve investigation on sensitivity of the results on the chemical mechanism. Nevertheless, the PANS model exhibited highly remarkable overall performance. Hence, it can be concluded that PANS turbulence model has potential do deliver accurate results under computational expense affordable for today's industrial standards. Following this conclusion, the PANS model can be employed to investigate high pressure fuel injection and combustion process in dual fuel configuration.

ACKNOWLEDGMENTS

This work has received funding from the European Union's Horizon 2020 research and innovation programme under the Marie Sklodowska-Curie grant agreement No 861002.

DECLARATION

The authors declare that the article has not been published elsewhere and that it has not been simultaneously submitted for publication elsewhere.

Nomenclature

χ_Φ	Scalar dissipation rate, (-)
Δ	Mesh size, (m)
δ_{ij}	Kronecker delta, (-)
ϵ_u	Unresolved eddy dissipation, (m^2/s^3)
Λ	Integral length scale, (m)
ν	Kinematic viscosity, (m^2/s)
ν_t	Turbulent viscosity, (m^2/s)
ν_{opt}	Optimized turbulent viscosity, (m^2/s)
ω	Source term, (-)
ϕ	Progress variable or mixture fraction scalar, (-)
ρ	Density, (kg/m^3)
τ_{ij}	Tangential stress tensor, (N/m^2)
ζ	Velocity scale ratio, (-)
C_{CSM}	Coherent structure model constant, (-)
D	Laminar diffusion coefficient of the fuel species, (-)
D_T	Turbulent diffusion coefficient of the fuel species, (-)
E	Velocity gradient tensor, (1/s)
f	Elliptic relaxation function, (-)
f_k	PANS Resolution parameter, (-)
F_Ω	Energy decay function, (-)

1	F_{CS}	Coherent structure function, (-)
2	k	Turbulent kinetic energy, (m^2/s^2)
3	k_u	Unresolved turbulent kinetic energy, (m^2)
4	k_{ssv}	Scale supplying variable, (m^2/s^2)
5	k_{tot}	Total turbulent kinetic energy, (m^2/s^2)
6	p	Pressure, (Pa)
7	P_k	Production of turbulent kinetic energy, (m^2/s^2)
8	PV	Mixture fraction, (-)
9	PV	Progress variable, (-)
10	Q	Second invariant of the velocity flow field, (-)
11	S_{ij}	Velocity strain tensor, (1/s)
12	T	Temperature, (K)
13	t	Time, (s)
14	u_i	Velocity component in direction i, (m/s)
15	W_{ij}	Vorticity tensor, (1/s)
16	x_i	Position vector, (-)

17 **REFERENCES**

18 Alla, G., Badr, O., Soliman, H., and Abd rabbo, M., Technical note: Exhaust emissions from an indirect
19 injection dual-fuel engine, *Proceedings of The Institution of Mechanical Engineers Part D-journal of*
20 *Automobile Engineering - PROC INST MECH ENG D-J AUTO*, vol. **214**, pp. 333–340, 2000.

21 Basara, B., Krajnović, S., Girimaji, S., and Pavlovic, Z., Near-wall formulation of the partially averaged
22 navier-stokes turbulence model, *AIAA Journal*, vol. **49**, pp. 2627–2636, 2011.

Basara, B., Pavlovic, Z., and Girimaji, S., A new approach for the calculation of the cut-off resolution parameter in bridging methods for turbulent flow simulation, *International JournaECI of Heat and Fluid Flow*, vol. **74**, pp. 76–88, 2018.
URL https://www.sciencedirect.com/science/article/pii/S0142727X18303199

Basara, B., Pavlovic, Z., and Girimaji, S.S., Multidimensional modeling of injection and combustion phenomena in a diesel ignited gas engine, Vol. 2017-March, SAE International, 2017.

ECN, Engine combustion network, , 2023.
URL https://ecn.sandia.gov/

(ECN), E.C.N., Modeling standards and recommendations, , 2022.
URL https://ecn.sandia.gov/diesel-spray-combustion/computational-method/odeling-standards

Eder, L., Ban, M., Pirker, G., Vujanovic, M., Priesching, P., and Wimmer, A., Development and validation of 3d-cfd injection and combustion models for dual fuel combustion in diesel ignited large gas engines, *Energies*, vol. **11**, p. 643, 2018.

Ferziger, J.H. and Peric, M., *Computational Methods for Fluid Dynamics*, Springer, 2002.

Fink, C., A Multi-Component Evaporation Model for 3D CFD-Code Fire 8: Development and Validation with Experimental Data, PhD thesis, Technical University of Graz, 2005.

FIRE^{TM}, A., 2022a. The TABKIN^{TM} FGM Model. AVL.

FIRE^{TM}, A., 2022b. The TABKIN^{TM} Table Generation Tool. AVL.

Gaballa, H., Modeling of dual-fuel jet break-up, phase change, and mixing, PhD thesis, Universite Paris-Saclay, 2023.

Gerard, D. and Lave, L.B., Implementing technology-forcing policies: The 1970 clean air act amendments and the introduction of advanced automotive emissions controls in the united states, *Technological Forecasting and Social Change*, vol. **72**, no. 7, pp. 761–778, 2005.
URL https://www.sciencedirect.com/science/article/pii/S0040162504001076

Girimaji, S. and Abdol-Hamid, K., Partially-averaged navier stokes model for turbulence: Implementation and validation, 2005.

Girimaji, S.S., Partially-Averaged Navier-Stokes Model for Turbulence: A Reynolds-Averaged Navier-Stokes to Direct Numerical Simulation Bridging Method, *Journal of Applied Mechanics*, vol. **73**,

no. 3, pp. 413–421, 2005.
URL https://doi.org/10.1115/1.2151207

Girimaji, S.S., Srinivasan, R., and Jeong, E., PANS Turbulence Model for Seamless Transition Between RANS and LES: Fixed-Point Analysis and Preliminary Results, Vol. Volume 2: Symposia, Parts A, B, and C of *Fluids Engineering Division Summer Meeting*, pp. 1901–1909, 2003.
URL https://doi.org/10.1115/FEDSM2003-45336

Hanjalic, K., Popovac, M., and Hadžiabdić, M., A robust near-wall elliptic-relaxation eddy-viscosity turbulence model for cfd, *International Journal of Heat and Fluid Flow*, vol. **25**, pp. 1047–1051, 2004.

Hooftman, N., Messagie, M., Van Mierlo, J., and Coosemans, T., A review of the european passenger car regulations – real driving emissions vs local air quality, *Renewable and Sustainable Energy Reviews*, vol. **86**, pp. 1–21, 2018.
URL https://www.sciencedirect.com/science/article/pii/S1364032118300182

Jakirlic, S., Chang, C.Y., and Basara, B., Computation of ic-engine-type flows by a variable resolution model, 2012, int. Multidimensional Engine Modeling (IMEM) User's Group Meeting at the SAE Congress, IMEM ; Conference date: 24-04-2012 Through 26-04-2012.

Klein, M., Ketterl, S., and Hasslberger, J., Large eddy simulation of multiphase flows using the volume of fluid method: Part 1—governing equations and a priori analysis, *Experimental and Computational Multiphase Flow*, vol. **1**, pp. 130–144, 2019.

Kobayashi, H., The subgrid-scale models based on coherent structures for rotating homogeneous turbulence and turbulent channel flow, *Physics of Fluids*, vol. **17**, no. 4, 2005, 045104.
URL https://doi.org/10.1063/1.1874212

Kobayashi, H., Ham, F., and Wu, X., Application of a local sgs model based on coherent structures to complex geometries, *International Journal of Heat and Fluid Flow*, vol. **29**, pp. 640–653, 2008.

Krajnović, S., Lárusson, R., and Basara, B., Superiority of pans compared to les in predicting a rudimentary landing gear flow with affordable meshes, *International Journal of Heat and Fluid Flow*, vol. **37**, p. 109–122, 2012.

Lapointe, S., Zhang, K., and McNenly, M., Reduced chemical model for low and high-temperature oxidation of fuel blends relevant to internal combustion engines, *Proceedings of the Combustion*

Institute, vol. **37**, no. 1, pp. 789–796, 2019.
URL https://www.sciencedirect.com/science/article/pii/S1540748918303225

LLNL, Lawrence livermore national laboratory, , 2022.
URL https://combustion.llnl.gov/mechanisms/alkanes/n-dodecane

Murthi, A., Reyes, D.A., Girimaji, S., and Basara, B., Turbulent transport modelling for pans and other bridging closure approaches, *Proceedings of the V European Conference on Computational Fluid Dynamics ECCOMAS CFD 2010*, ., pp. ——, 2010, fifth European Conference on Computational Fluid Dynamics ECCOMAS CFD 2010 ; Conference date: 14-06-2010 Through 17-06-2010.

Perkovic, L., Numerical modelling of turbulent premixed jet flames in large eddy simulation framework, PhD thesis, Faculty of Mechanical Engineering and Naval Architecture, University of Zagreb, 2014.

Petranovic, Z., Numerical modelling of spray and combustion processes using the Euler Eulerian multi-phase approach, PhD thesis, Faculty of Mechanical Engineering and Naval Architecture, University of Zagreb, 2016.

Popovac, M. and Hanjalic, K., Compound wall treatment for rans computation of complex turbulent flows and heat transfer, *Flow, Turbulence and Combustion*, vol. **78**, 2007.

Przulj, V. and Basara, B., 2001. Bounded convection schemes for unstructured grids.
URL https://arc.aiaa.org/doi/abs/10.2514/6.2001-2593

Reitz, R., Modeling atomization processes in high-pressure vaporizing sprays, *Atomisation Spray Technology*, vol. **3**, pp. 309–337, 1987.

Reyes, D., Cooper, J., and Girimaji, S., Characterizing velocity fluctuations in partially resolved turbulence simulations, *Physics of Fluids*, vol. **26**, p. 085106, 2014.

Schlatter, S., Schneider, B., Wright, Y., and Boulouchos, K., Experimental study of ignition and combustion characteristics of a diesel pilot spray in a lean premixed methane/air charge using a single stroke machine, *SAE Technical Paper No. 2012-01-0825*, 2012.

Sweby, P.K., High resolution schemes using flux limiters for hyperbolic conservation laws, *SIAM Journal on Numerical Analysis*, vol. **21**, no. 5, pp. 995–1011, 1984.
URL https://doi.org/10.1137/0721062

Tazraei, P. and Girimaji, S., Scale-resolving simulations of turbulence: Equilibrium boundary layer analysis leading to near-wall closure modeling, *Physical Review Fluids*, 2019.

Tvrdojevic, M., Vujanovic, M., Priesching, P., Tap, F., Starikov, A., Goryntsev, D., and Gavaises, M., Implementation of the semi empirical kinetic soot model within chemistry tabulation framework for efficient emissions predictions in diesel engines, *Open Physics*, vol. **17**, pp. 905–915, 2019.

van Oijen, J., Donini, A., Bastiaans, R., ten Thije Boonkkamp, J., and de Goey, L., State-of-the-art in premixed combustion modeling using flamelet generated manifolds, *Progress in Energy and Combustion Science*, vol. **57**, pp. 30–74, 2016.
URL https://www.sciencedirect.com/science/article/pii/S0360128515300137

Xu, C., Zhuang, Y., Qian, Y., and Cho, H., Effect on the performance and emissions of methanol/diesel dual-fuel engine with different methanol injection positions, *Fuel*, vol. **307**, p. 121868, 2022.
URL https://www.sciencedirect.com/science/article/pii/S0016236121017476

Xu, S., Zhong, S., Pang, K.M., Yu, S., Jangi, M., and Bai, X.S., Effects of ambient methanol on pollutants formation in dual-fuel spray combustion at varying ambient temperatures: A large-eddy simulation, *Applied Energy*, vol. **279**, p. 115774, 2020.

Xue, Q., Battistoni, M., Powell, C., Longman, D., Quan, S., Pomraning, E., Senecal, P., Schmidt, D., and Som, S., An eulerian cfd model and x-ray radiography for coupled nozzle flow and spray in internal combustion engines, *International Journal of Multiphase Flow*, vol. **70**, 2014.

Žilić, A., Large-Eddy Simulation of Fuel Injection at Subcritical and Supercritical Conditions, PhD thesis, Technischen Fakultät der Friedrich-Alexander-Universität Erlangen-Nürnberg, 2021.

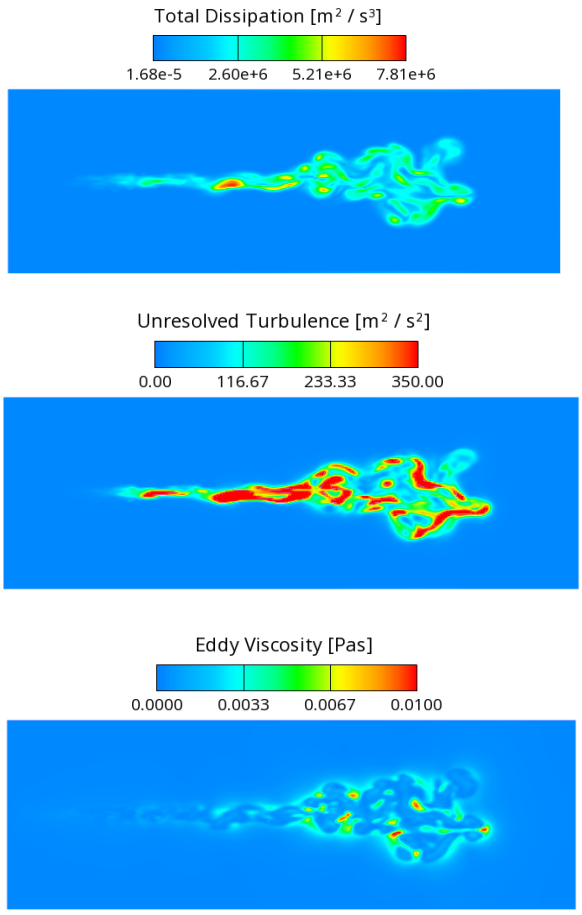

FIG. 1: Total eddy dissipation, unresolved turbulence and turbulent eddy viscosity as obtained by coherent structure model in case of high-pressure liquid injection process.

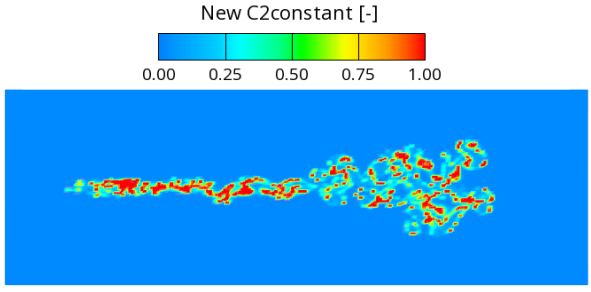

FIG. 2: Distribution of calculated values for the C_2 constant of the coherent structure subgrid model.

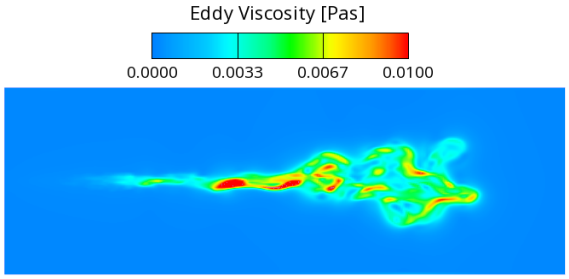

FIG. 3: Turbulent eddy viscosity as obtained by Eq. 12.

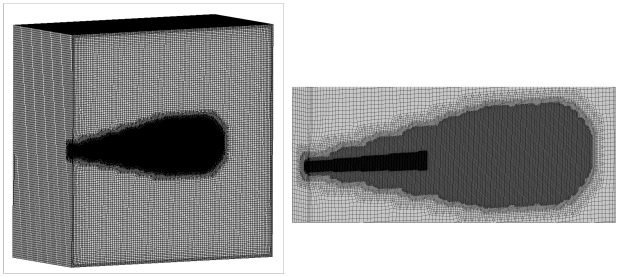

FIG. 4: Computational domain used for the CFD simulation with a zoom on spray area

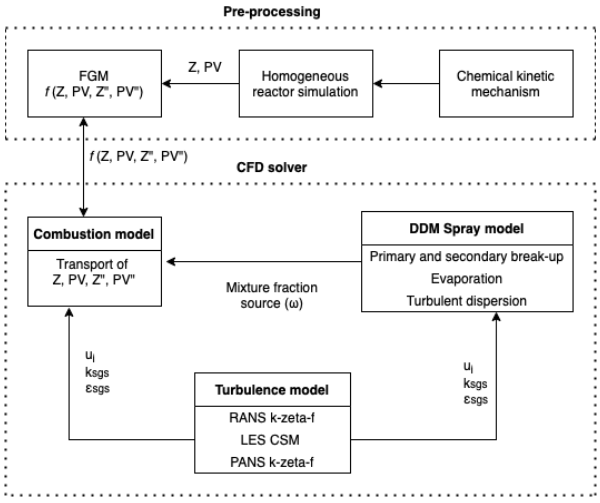

FIG. 5: Employed simulation workflow scheme.

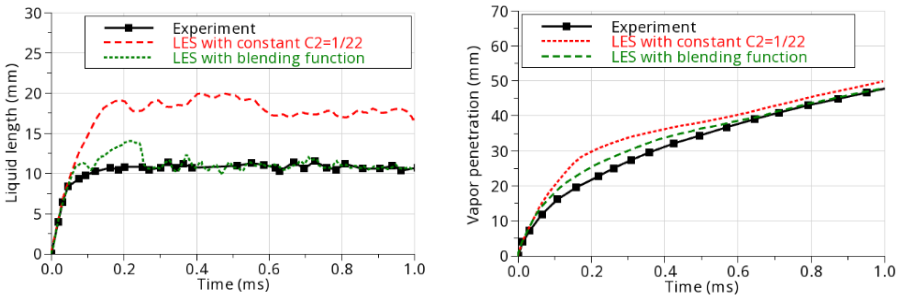

FIG. 6: Comparison of liquid length (left) and vapor penetration (right) obtained from LES simulation utilizing the blending function to experimental data and numerical results obtained utilizing original LES coherent structure model.

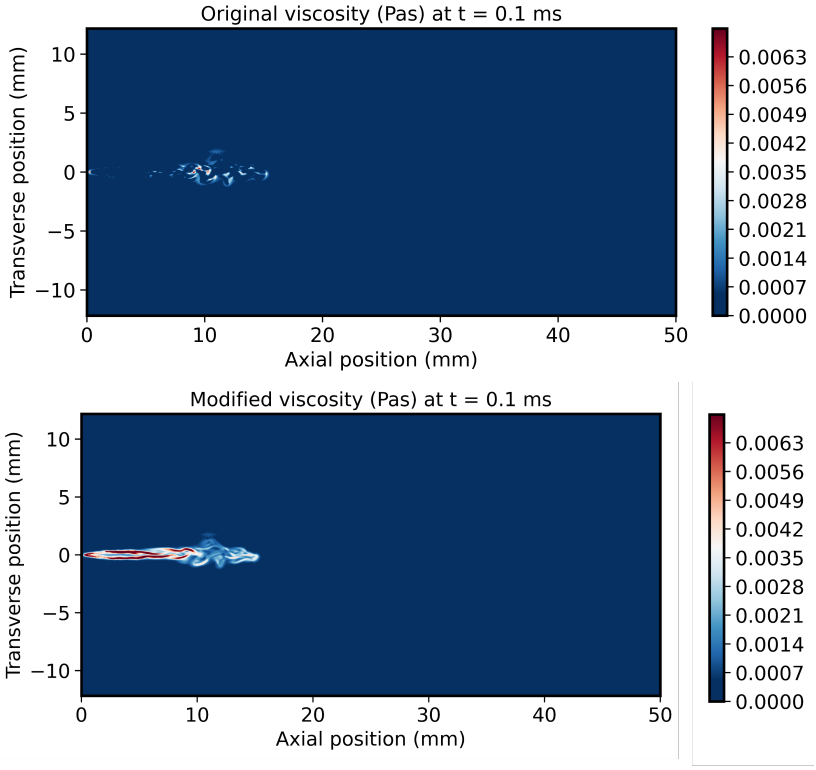

FIG. 7: Turbulent eddy viscosity as predicted by the original formulation of the LES CSM model with the constant value of $C_2 = 1/22$ (upper figure), compared to the eddy viscosity obtained from LES CSM model when the viscosity is blended between viscosity near wall, with $C_2 = 1/22$ and viscosity in the turbulent region, with $C_2 = 1$ (lower figure). Time instance is 0.1 ms.

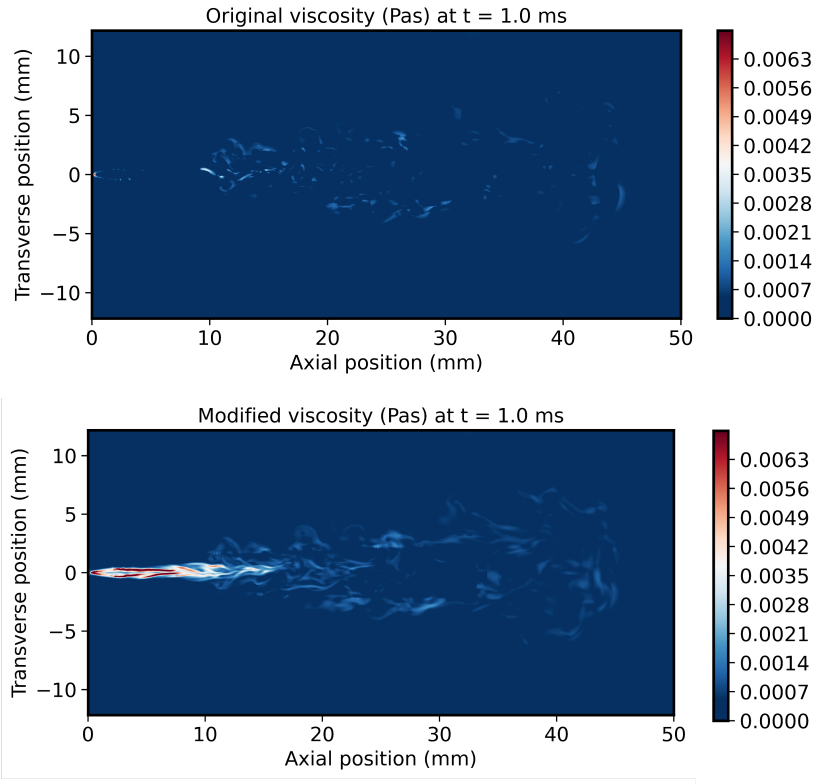

FIG. 8: Turbulent eddy viscosity as predicted by the original formulation of the LES CSM model with the constant value of $C_2 = 1/22$ (upper figure) , compared to the eddy viscosity obtained from LES CSM model when the viscosity is blended between viscosity near wall, with $C_2 = 1/22$ and viscosity in the turbulent region, with $C_2 = 1$ (lower figure). Time instance is 1 ms.

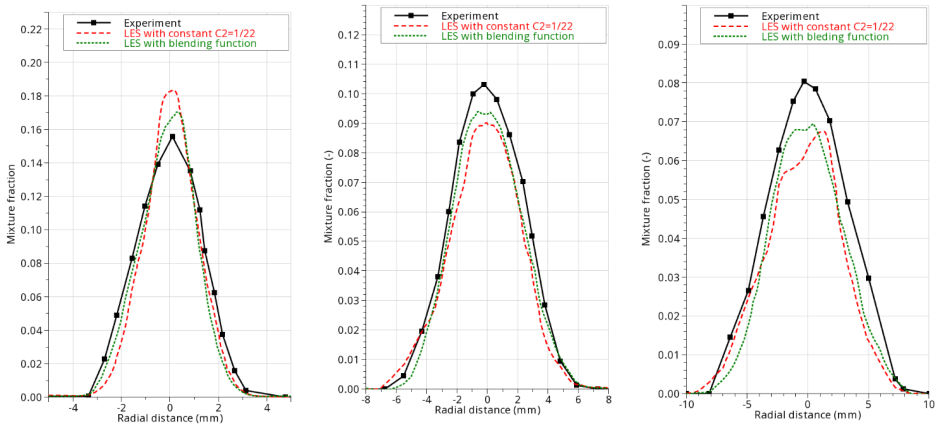

FIG. 9: Radial distribution of n-dodecane mass fraction at 18 mm from the nozzle exit (left), 30 mm from the nozzle exit (middle) and 40 mm from the nozzle exit (right). Comparison between experimental data, CFD results from LES simulation utilizing the blending function and original coherent structure model.

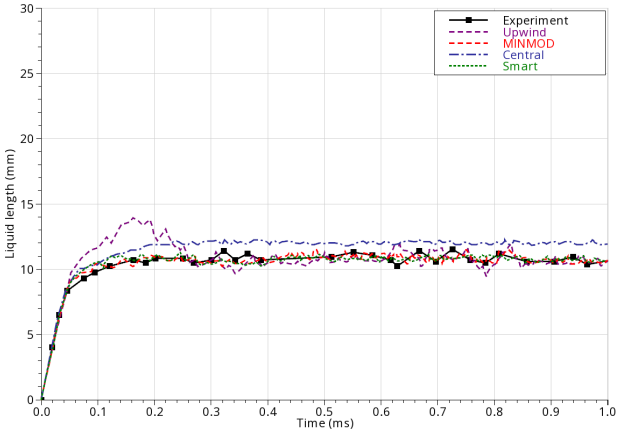

FIG. 10: Liquid length as obtained by PANS simulation employing upwind, MINMOD, AVL Smart and central differencing schemes for momentum compared to experimental data.

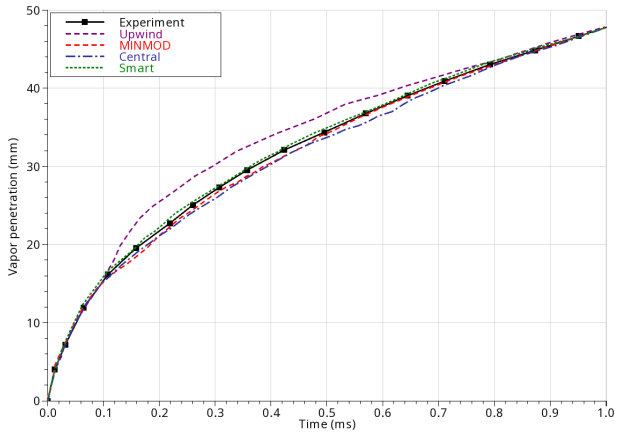

FIG. 11: Vapor penetration as obtained by PANS simulation employing upwind, MINMOD, AVL Smart and central differencing schemes for momentum compared to experimental data.

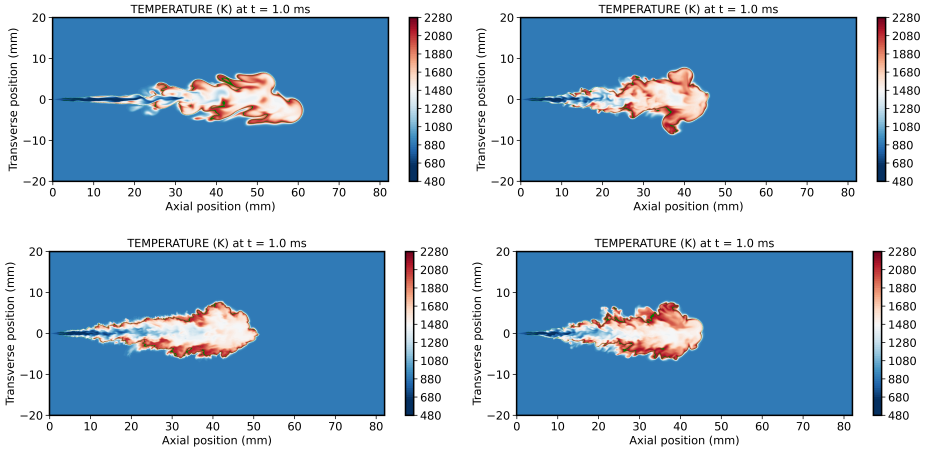

FIG. 12: Temperature distribution as obtained by PANS simulations utilizing Upwind (upper left), MINMOD (upper right), Central (lower left) and AVL Smart (lower right) differencing schemes.

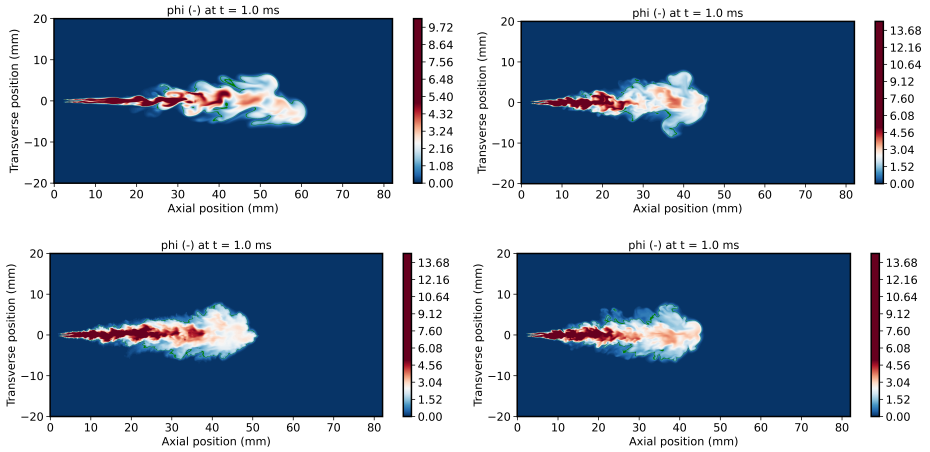

FIG. 13: Equivalence ratio distribution as obtained by PANS simulations utilizing Upwind (upper left), MINMOD (upper right), Central (lower left) and AVL Smart (lower right) differencing schemes.

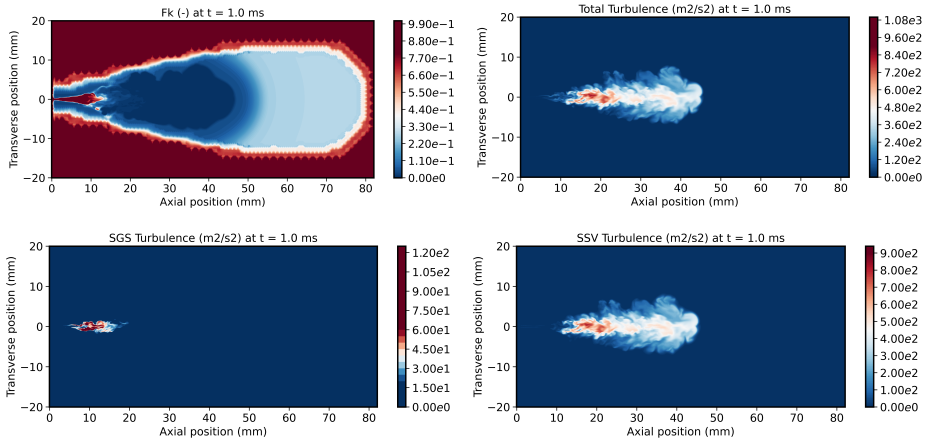

FIG. 14: Resolution parameter (upper left), total (upper right), unresolved (lower left) and resolved (lower right) turbulent kinetic energy as obtained by PANS turbulence model.

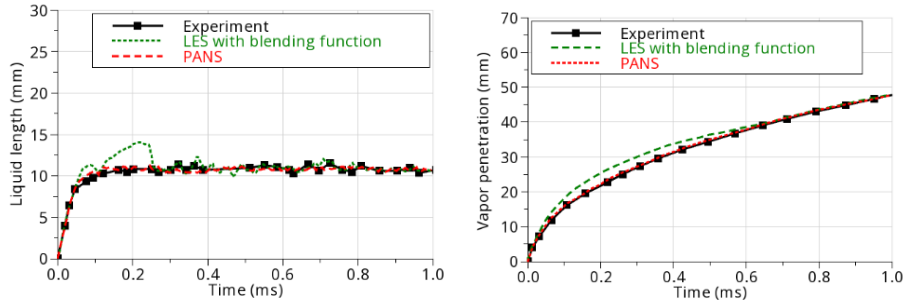

FIG. 15: Comparison of liquid length (left) and vapor penetration (right) predicted by LES coherent structure model with blending function and PANS $k - \zeta - f$ turbulence model.

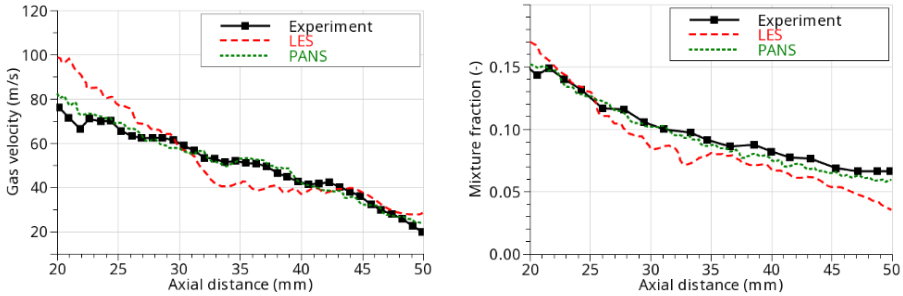

FIG. 16: Comparison of the results obtained with LES coherent structure model with blending function and PANS $k-\zeta-f$ turbulence model for gas velocity (left) and mixture fraction axial distribution (right).

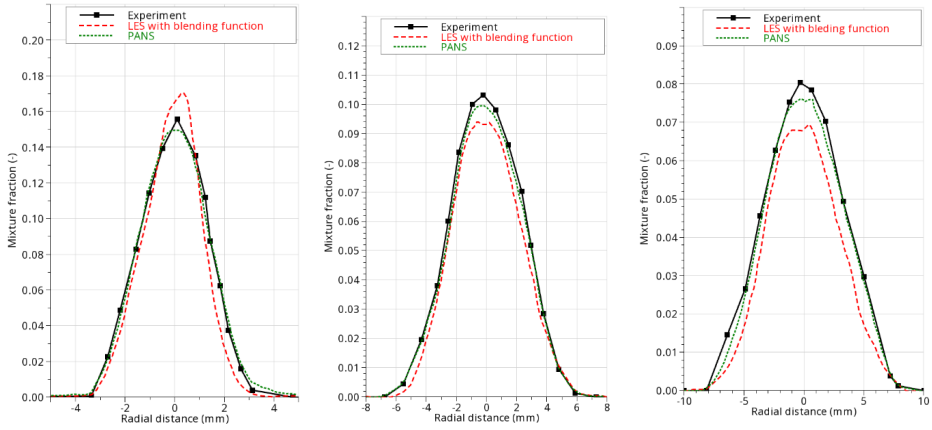

FIG. 17: Radial distribution of n-dodecane mass fraction at 18 mm from the nozzle exit (left) 30 mm from the nozzle exit (middle) and 40 mm from the nozzle exit (right). Comparison between experimental data, CFD results from LES simulation utilizing the blending function and PANS simulation.

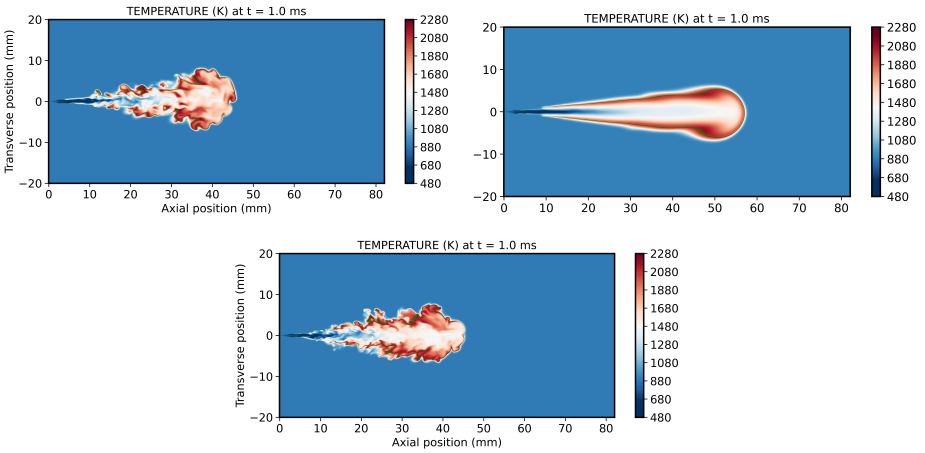

FIG. 18: Comparison of the temperature distribution as predicted by LES CSM with blended eddy viscosity (upper left), RANS $k-\zeta-f$ model (upper right)) and PANS $k-\zeta-f$ SSV model (lower).

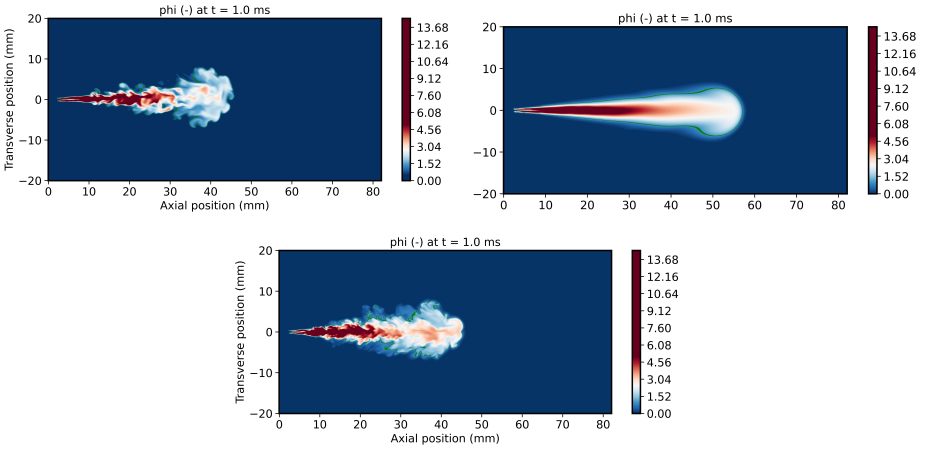

FIG. 19: Comparison of the equivalence ratio distribution as predicted by LES CSM with blended eddy viscosity (upper left), RANS $k-\zeta-f$ model (upper right) and PANS $k-\zeta-f$ SSV model (lower).

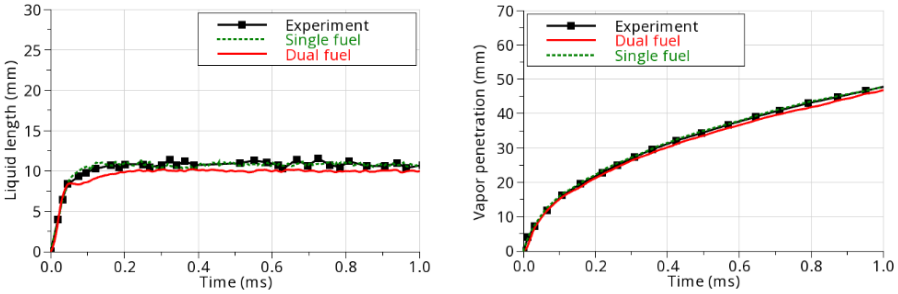

FIG. 20: Comparison of liquid length (left) and vapor penetration (right) between single fuel and dual fuel Spray A configuration.

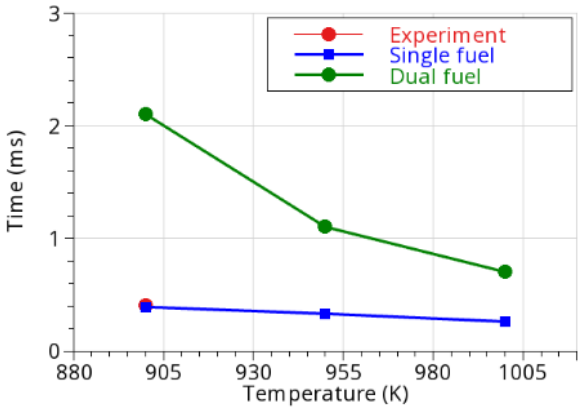

FIG. 21: Comparison of ignition delay time between single fuel and dual fuel configuration for three different temperatures.

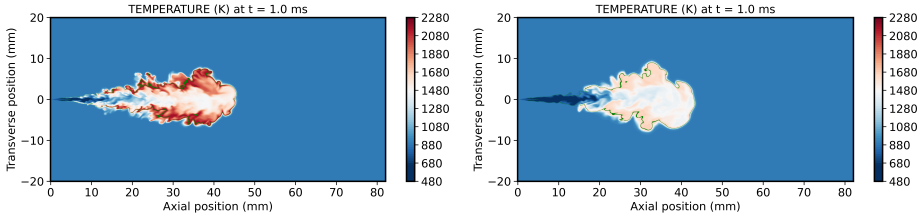

FIG. 22: Temperature distribution as obtained by PANS simulation for single fuel configuration (left) and dual fuel configuration (right).

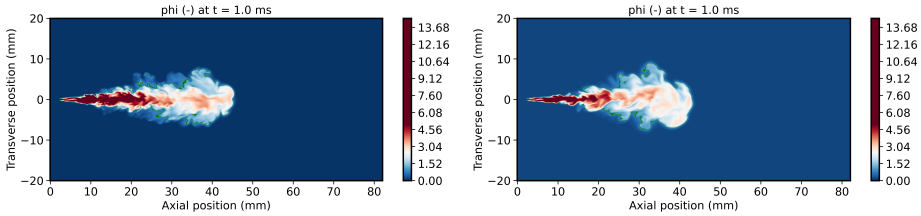

FIG. 23: Equivalence ratio distribution as obtained by PANS simulation for single fuel configuration (left) and dual fuel configuration (right).

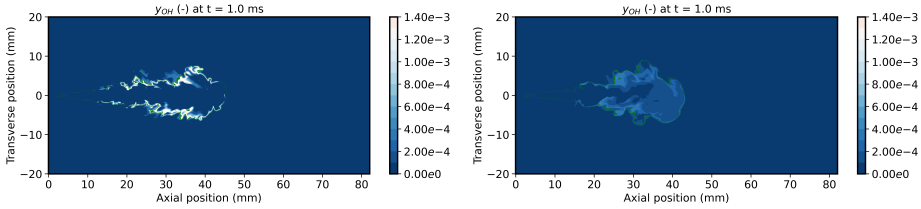

FIG. 24: OH mass fraction as obtained by PANS simulation for single fuel configuration (left) and dual fuel configuration (right).

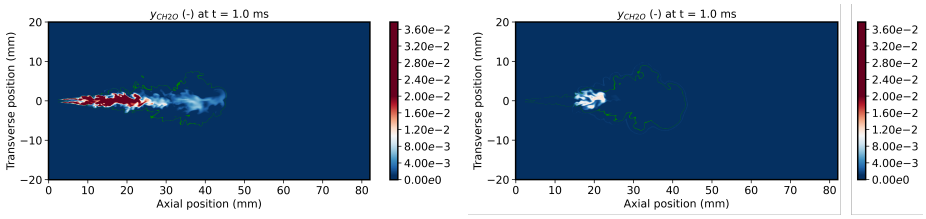

FIG. 25: HCOH mass fraction as obtained by PANS simulation for single fuel configuration (left) and dual fuel configuration (right).

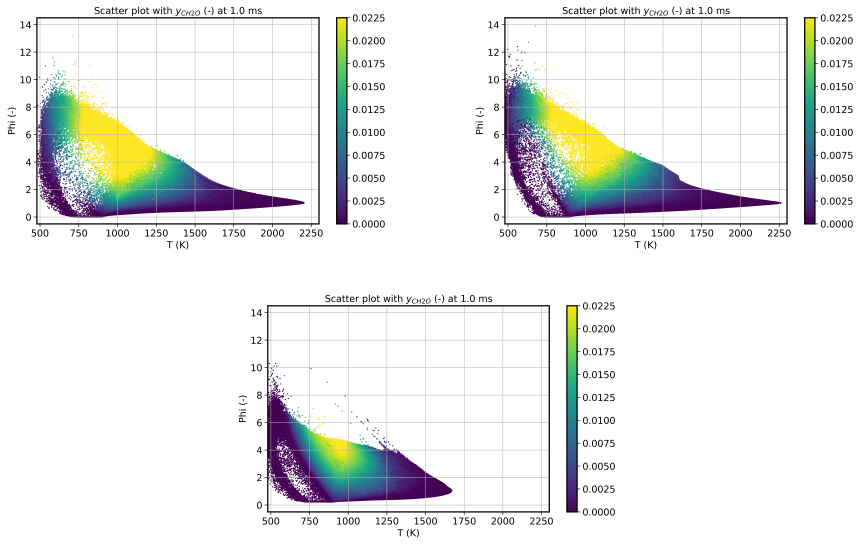

FIG. 26: HCHO scatter plots as predicted by PANS simulation for single fuel configuration (upper left), LES simulation for single fuel configuration (upper right) and PANS simulation for dual fuel configuration (lower).

Fuel	n-dodecane
Injection pressure	150 MPa
Injection temperature	363 K
Injection duration	1.5 ms
Number of nozzle holes	1
Ambient gas temperature	900 K
Ambient gas pressure	6 bar
Ambient gas density	22.8 kg/m^3

TABLE 1: ECN Spray A operating conditions as prescribed by ECN (2023)

Chemical mechanism	Hybrid reduced n-dodecane
Pressure	9 points from 1 to 80 bar
Temperature	22 points from 300 to 2000 K
Mixture fraction	55 points from 0 to 1
Progress variable	110 points from 0 to 1
Mixture fraction segregation	10 points from 0 to 1
Progress variable segregation	12 points from 0 to 1
Fuel ratio	6 points from 0 to 1

TABLE 2: FGM table discretization.